Received: 16 July 2013 Revised: 3 September 2013 Accepted article published: 11 September 2013 Published online in Wiley Online Library: 4 October 2013

(wileyonlinelibrary.com) DOI 10.1002/jctb.4220

Graphene oxide and its application as an adsorbent for wastewater treatment

George Z. Kyzas, Eleni A. Deliyanni* and Kostas A. Matis

Abstract

Graphene oxide, particularly as magnetic particles, has recently been used as an adsorbent for wastewater treatment in applications such as heavy metals separation (mercury, cadmium, copper, chromium, arsenic) and also organics (antibiotics, dyes, i.e. Reactive black 5, etc.). Selected examples will be given in the present review – mostly from the literature. The following themes are examined among others: the synthesis route (impregnation, co-precipitation), kinetics of adsorption, thermodynamics, isotherm studies and applications in comparison with other adsorbents.

Keywords: adsorption; nanoparticles; effluent treatment; heavy metals removal; dyes

INTRODUCTION

Even before physicists Andre K. Geim and Konstantin S. Novoselov of the University of Manchester (UK) were honoured with the 2010 Nobel Prize for their pioneering work with graphene, the range of graphene's potential applications discussed in scientific circles was impressively broad; it's even broader now.[1] A survey of today's graphene market showed that a couple of small companies have been selling microscopic amounts of graphene flakes for a few years, mainly to academic researchers for fundamental investigations. Also, the application of nanotechnology has significantly expanded in a great diversity of industrial sectors (and research groups) in order to enhance processes or develop new ones, as nanoparticles have distinctive characteristics.[2] Graphene and its derivatives have been examined for pollution management, for instance gas adsorption.[3] The incorporation of graphene oxide in the usual adsorbents, like chitosan, increased its compressive strength, and produced an efficient and biodegradable monolith.[4]

The large-scale production of functionalized graphene at low cost should result in good adsorbents for water purification.[3] This is due to the two-dimensional layer structure, large surface area, pore volume and presence of surface functional groups in these materials; the inorganic nanoparticles also prevent aggregation of the adsorbent. Water, as is known (from several good handbooks), can be treated and purified by multiple techniques, such as desalination, filtration, membranes, flotation, adsorption, disinfection, sedimentation. Certainly, adsorption has advantages over other methods (some of these will be shown in the following), such as for example ease of operation and comparatively low cost. Adsorption is the surface phenomenon whereby pollutants are adsorbed onto the surface of a material (adsorbent) via physical and/or chemical forces. It depends on many factors such as temperature, solution pH, concentration of pollutants, contact time, particle size, temperature, nature of the adsorbate and adsorbent, etc.

The aim of the present review is to develop and comment on the recent applications of graphene oxide (denoted hereafter as GO) as an adsorbent for wastewater treatment. This study includes a brief introduction to adsorption data (isotherms, thermodynamics and kinetics) and some crucial points for the preparation routes of graphene oxides (i.e. nanocompsites, magnetic materials, etc.). Characterization of the prepared adsorbents is also commented on, in line with detailed recent data about the use of GO for the removal of organics (i.e. dyes, antibiotics) and heavy metals from wastewaters.

ADSORPTION (ISOTHERMS, THERMODYNAMICS AND KINETICS)

The capacity of an adsorbent can be described by the equilibrium adsorption isotherm, which is characterized by certain constants whose values express the surface properties and affinity of the adsorbent. The adsorption isotherm is important from both theoretical and practical points of view. The parameters obtained from the different models provide important information about the adsorption mechanism, the surface properties and the affinities of adsorbents. Among the isotherm equations available for analyzing experimental adsorption equilibrium data, the most widely used adsorption models for single-solute systems are the Freundlich and Langmuir models. The Freundlich isotherm is expressed as follows:[5]

$$q_e = K_F C_e^{1/n} \quad (1)$$

The saturated monolayer isotherm (Langmuir equation) is represented as follows:[6]

$$q_e = \frac{q_{max} b\, C_e}{1 + b\, C_e} \quad (2)$$

* *Correspondence to: Eleni A. Deliyanni, Division of Chemical Technology & Industrial Chemistry, Department of Chemistry, Aristotle University of Thessaloniki, GR-541 24 Greece. E-mail: lenadj@chem.auth.gr*

Division of Chemical Technology & Industrial Chemistry, Department of Chemistry, Aristotle University of Thessaloniki, GR-54124 Greece

where q_e (mg g^{-1}) is the equilibrium concentration of pollutant in the solid phase; K_F ($mg^{1-1/n}$ $L^{1/n}/g$) is the Freundlich constant representing the adsorption capacity; C_e (mg L^{-1}) is the equilibrium concentration of pollutant in the liquid phase; n (dimensionless) is the constant depicting the adsorption intensity; q_{max} (mg g^{-1}) is the maximum amount of adsorption; b (L mg^{-1}) is the Langmuir adsorption equilibrium constant.

The Freundlich isotherm model, which is empirical, generally is applied to adsorption on heterogenous surfaces, with the interaction among adsorbed molecules. The application of this equation also suggests that the adsorption energy decreases exponentially on completion of the adsorption centers of an adsorbent. The isotherm can be used for non-ideal adsorption, where K_F in the model is the Freundlich constant related to the bonding energy. This can be defined as an adsorption or distribution coefficient and represents the adsorption capacity (i.e. quantity adsorbed onto the adsorbent for unit equilibrium pollutant concentration), while the exponent '1/n' is the heterogeneity factor, and n is a measure of the deviation from linearity of adsorption. Its value indicates the degree of non-linearity between solution concentration and adsorption as follows: if the value is below unity, then the adsorption process is chemical; however, if the value is above unity, adsorption is a favourable physical process.

The Langmuir isotherm, on the other hand, assumes monolayer coverage of adsorbate over a homogenous adsorbent surface, and the adsorption of each molecule onto the surface has the same activation energy of adsorption. In this isotherm model, q_{max} is the maximum adsorption capacity reflected to a complete monolayer coverage and b is an affinity constant related to the energy of adsorption. The value of b indicates the strength or affinity of the adsorbate for the solute.

The Gibbs free energy change (ΔG^0, kJ mol^{-1}) of the adsorption process is expressed by the Van't Hoff equation (Equation 3),[7] with the previous calculation of the equilibrium constant (K_0):

$$\Delta G^0 = -R\ T\ \ln(K_0) \tag{3}$$

where T (K) is the temperature and R (=8.314 J mol^{-1} K) is the universal gas constant.

The change in entropy (ΔS^0, kJ mol^{-1} K) and the heat of adsorption (ΔH^0, kJ mol^{-1}) at a constant temperature T (K) can be calculated from Equation 4:

$$\Delta G^0 = \Delta H^0 - T\Delta S^0 \tag{4}$$

The isosteric heat of adsorption (ΔH_x) is calculated using the Clausius–Clapeyron equation given by the following formula:

$$\Delta H_x = 2.303 \times R \times \left(\log\left(C_{e_1}\right) - \log\left(C_{e_2}\right)\right) \times \left(\frac{T_1 T_2}{T_2 - T_1}\right) \tag{5}$$

The thermodynamic equilibrium constant (K_0) for the process is determined by plotting $\ln(q_e/C_e)$ versus q_e, and extrapolating to zero q_e using a graphical method; regression straight lines are usually fitted through the data points by the least squares method. The intersection with the vertical axis gives the value of K_0. Values of ΔS^0 and ΔH^0 are evaluated from the slope and intersect of the van't Hoff plots. The isosteric heat of adsorption (ΔH_x) is calculated using the intergrated form of the Clausius–Clapeyron equation (Equation 5). The aforementioned parameter is estimated by using the linearized form of the Freundlich equation.

For a constant q_e value, at different temperatures, the respective equilibrium concentrations of solute in the solution ($\log(C_e)$) are estimated. ΔH_x was the mean value of three calculations for three pairs of different temperatures. The values of ΔH obtained using these two methods were almost equal.[8]

Adsorption kinetics may be controlled by several independent processes which can act in series or parallel.[9] These processes fall into one of the following general categories: (i) bulk diffusion; (ii) external mass transfer (film diffusion); (iii) chemical reaction (chemisorption); and (iv) intraparticle diffusion.

Kinetic analyses not only allow estimation of adsorption rates but also lead to suitable rate expressions characteristic of possible reaction mechanisms. Nevertheless, the conclusion, in the example of metals biosorption thoroughly studied, was that the analysis conducted had not been capable of providing strong evidence in favour of any of the mechanisms examined, since several diverse kinetic models were successful in fitting the experimental data.[9]

It was also said[10] that the pseudo-second-order equation (which implies that one adsorbate specie occupies two binding sites) may be applied for chemisorption processes with a high degree of correlation in several literature cases, where a pseudo-first-order rate mechanism was arbitrarily assumed. This equation for the time over the rate of adsorption (Q_t) becomes:

$$\frac{t}{Q_t} = \frac{1}{k_2 Q_e^2} + \left(\frac{1}{Q_e}\right) t \tag{6}$$

where k_2 (g mg^{-1} min^{-1}) is the reaction rate constant; Q_e (mg g^{-1}) is the equilibrium adsorption capacity, and t (min) is the contact time between adsorbent and adsorbate solution. However, it was reported that the pseudo-second-order process is followed when the initial solute concentration is not too high, otherwise it is pseudo-first-order.[11]

MATERIALS SYNTHESIS

Wang and co-workers[12] reviewed the main routes of GO preparation: chemical oxidation and exfoliation of graphite using either the Brodie, Staudenmaier, or Hummers method, or some variations of these methods. Brodie first found that the oxidizing mixture ($KClO_4$ with fuming HNO_3) could form GO only with graphitizable carbons that contain regions of graphitic structure.[13] Staudenmaier then reported the formation of GO when graphite was heated with H_2SO_4, HNO_3, and $KClO_4$.[14] Later, Hummers and Offeman introduced a convenient method to prepare GO using H_2SO_4 and $KMnO_4$.[15]

In the present review the GO adsorbents which will be reviewed/commented were synthesized according to the modified Hummers method.[15] In a typical procedure, 120 mL of concentrated H_2SO_4 were added into a 500 mL flask containing 5 g of graphite and followed by stirring for 30 min in an ice bath. Then, 15 g of $KMnO_4$ were added slowly to the mixture. The rate of addition was carefully controlled to maintain the reaction temperature below 20°C. The mixture was stirred at room temperature overnight. Then, 150 mL of H_2O were slowly added under vigorous stirring. The reaction temperature rapidly increased to 98°C, and the color of the mixture changed to yellow. The diluted suspension was stirred at 98°C for 24 h and 50 mL of H_2O_2 (30% v/v) were then added to the mixture. For purification, the mixture was washed by rinsing and centrifugation

with HCl (5% v/v) followed by deionized water several times. After filtration and freeze drying, graphite oxide was obtained as a solid.

Fe_3O_4/GO nanocomposites were prepared by two different routes: (i) impregnation (denoted as mGOi); and (ii) co-precipitation (denoted as mGOp).[16] Fe_3O_4 nanoparticles were prepared according to the modified Massart method[17] via the co-precipitation of a mixture of $FeCl_3 \cdot 6H_2O$ and $FeCl_2 \cdot 4H_2O$. In particular, $FeCl_3 \cdot 6H_2O$ (3.03 g, 11.2 mmol) and $FeCl_2 \cdot 4H_2O$ (1.13 g, 5.6 mmol) were completely dissolved in 150 mL of deionized water. The aqueous solution was heated to 60°C, in order to obtain a clear yellow solution under vigorous agitation. Then, aqueous ammonia solution was added dropwise until the pH of the solution reached 10. The reaction was maintained for an additional 30 min under vigorous stirring. Nitrogen was used as the protective gas throughout the experiment. After completion of the reaction, the black precipitate was collected by an external magnetic field, followed by washing several times with deionized water and ethanol. Finally, the Fe_3O_4 nanoparticles were freeze-dried.

In a typical synthesis of Fe_3O_4/GO nanocomposites by co-precipitation (mGOp), GO (0.3 g) was dispersed in 150 mL water by sonication for 30 min in order for GO to be formed. Then, 0.825 g of $FeCl_3 \cdot 6H_2O$ and 0.322 g of $FeCl_2 \cdot 4H_2O$ were dissolved in 25 mL of water and the solution was added dropwise to GO solution at room temperature under a nitrogen flow with vigorous stirring. After completing ion exchange, ammonia solution (28% v/v) was added dropwise to make the pH of solution equal to 10 for synthesis of magnetite nanoparticles. The temperature of the solution increased to 80°C. After stirring for about 45 min, the black precipitate was centrifuged, washed with ethanol several times, and finally freeze-dried.

For the synthesis of Fe_3O_4/GO nanocomposites by impregnation (mGOi), the graphite oxide dispersion (0.3 g GO in 300 mL distilled water) was sonicated for 30 min in order for GO to be formed. An amount of Fe_3O_4 nanoparticles (0.3 g) was added to the dispersion. After 30 min of sonication, to obtain a homogenous suspension, the resulting nanocomposites were collected by centrifuging and then freeze-dried.

The use of magnetic materials in solid phase extraction has received considerable attention, taking into account the advantages arising from the inherent characteristics of magnetic particles.[18] The methodology overcomes problems such as column packing and phase separation, which can be performed by applying an external magnetic field. The most important factor for successful separation is the choice of the appropriate magnetic adsorbent material which dominates the selectivity and sensitivity of the method. In fact, this separation technique has long been applied in mineral processing, for instance the magnetic separation of wolframite–cassiterite in the South Crofty mine in Cornwall (UK) and the magnesite ores in Gerakini (Chalkidiki, Greece). Both were visited by one of the authors (Professor K.A. Matis).

Elsewhere, a facile synthetic route for the preparation of reduced graphene oxide (RGO)-metal/metal oxide composites was reported.[19] The method was found to be versatile and applicable for the syntheses of a variety of RGO-composites; their application in water purification was examined. A redox-like reaction between RGO and metal precursor was the major cause for composite formation. As the metal precursors were being reduced, RGO was becoming progressively oxidized primarily to GO and the metal nanoparticles formed were closely anchored onto the carbon sheets. Despite its first experimental synthesis more than 150 years ago, the structure of GO is still elusive today due to its non-stoichiometry. So far, several models have been proposed to elucidate its structure.[20]

A goal of another work was to fabricate and characterize a novel magnetic composite of GO and polystyrene.[21] Fabrication was achieved through two steps: (i) an effective one-pot co-precipitation of iron (II) and (III) chlorides, in the presence of graphene oxide, which resulted in the fabrication of magnetite–GO hybrid-nanoparticles; and (ii) loading of the latter over polystyrene through *in situ* emulsion polymerization afforded the magnetic composite. Knowledge of the properties and applications of this composite was stated to be at an embryonic stage.

Carbon materials have also been impregnated into TiO_2 photocatalysts and have become a research focus since pure TiO_2 has limited adsorption and photocatalytic ability (i.e. of dyes; P25 (of Degussa)). Graphene nanocomposite photocatalyst was prepared by hydrothermal methods.[22]

Chitosan is a multifunctional polymer that has primary and secondary hydroxyl groups, as well as highly reactive amino groups. It has been regarded as a useful starting support for adsorption purposes. Numerous investigations of the chemical activation of chitosan have been carried out to increase its adsorption capacity for metals. In the past, magnetic chitosan has emerged as a new generation of materials for environmental decontamination.[23]

Mercury (one of the most toxic heavy metals) ions and a commercial reactive dye (anionic and anthraquinonic) were tried as target molecules for classical adsorption experiments. The former's presence is due to a combination of natural processes (volcanic action, erosion of mercury-containing sediments) and anthropogenic activities (mining operations, tanneries, metal plating facilities). Contamination of aquatic systems is certainly a serious environmental problem given the pollution of natural waters by heavy metal ions.

The reactive dye, Reactive Black 5 – C.I. 20505 (abbreviated as RB5, supplied by Kahafix), presents the following characteristics: $C_{26}H_{21}N_5Na_4O_{19}S_6$, M.W. = 991.82 g mol^{-1}, λ_{max} = 603 nm, purity = 55% w/w. The chemical structure of the dye used is also given in Fig. 1. The dyeing process of cotton textiles using reactive dyes (cotton fibers make up about half of the worldwide consumption of fibers) involves unit operations such as desizing, scouring, bleaching, dyeing and finishing. The waste streams from each individual sub-operation are collected to an 'equalization tank', where they are mixed and homogenized.[24]

CHARACTERIZATION

Insights into the structure of GO (and RGO) are of significant interest, as their properties are dependent on the type and distribution of functional groups, defects, and holes from missing carbons in the GO carbon lattice.[20] Major functional groups in GO are epoxy, hydroxyl, and carbonyl, which locate on the basal plane of the carbon skeleton, and carboxyl, which sits on the edge. Epoxies are energetically favourable to sit above the bridge site and are randomly distributed in close proximity with hydroxyl to stabilize the structure, while carbonyls lie in the plane on average. Tiny islands of pure epoxies and hydroxyls also exist in the carbon network. In addition, graphene-like regions and holes are also common in GO. Modeling the structural motifs of GO can predict the structural evolution in

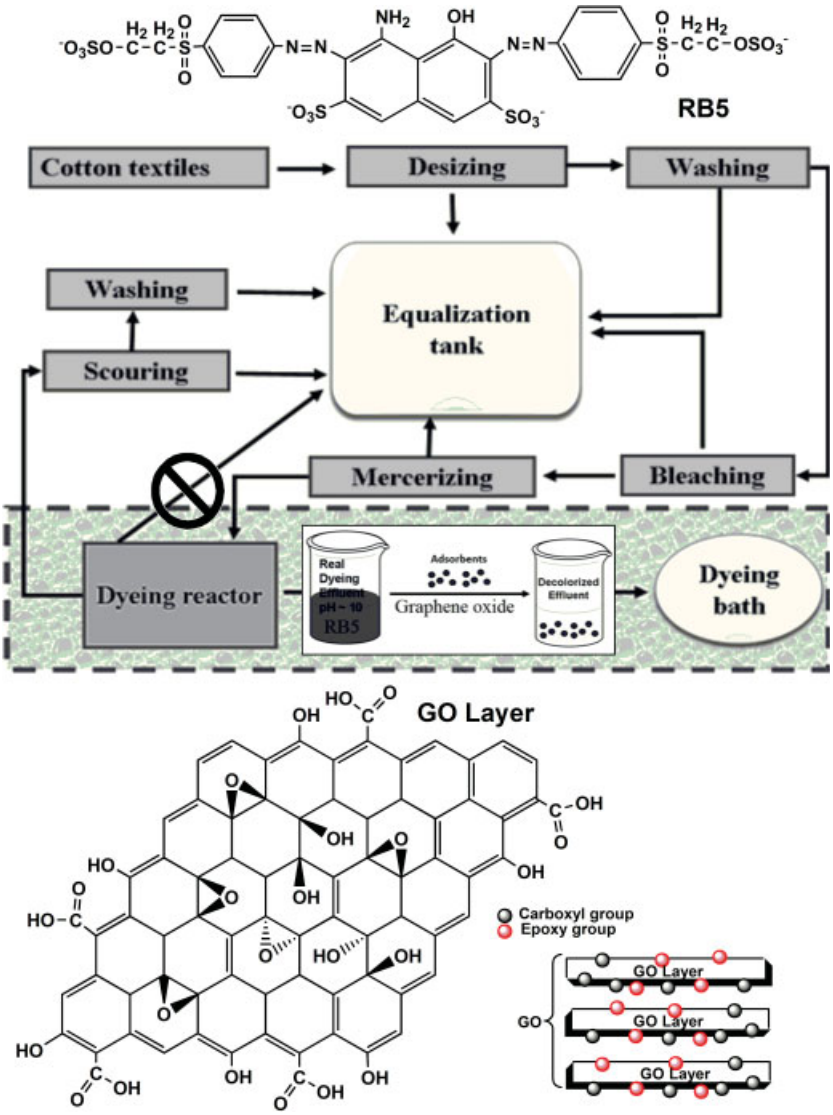

Figure 1. Illustrative scheme of the dyeing process and the proposed treatment of its effluents; RB5 dye (top) and functionalized GO adsorbent (bottom).

its reduction and presents promising directions to tailor the properties.

X-ray diffraction measurements (XRD) were performed in order to obtain crystalline structural information for magnetic composites prepared in our laboratory following the two aforementioned preparation routes (impregnation and co-precipitation). The characterization measurements for the prepared (and studied in the lab) mGOi and mGOp nanocomposites were presented in a series of figures;[17] the XRD patterns of the parent graphite and the graphite oxide were also presented. The sharp d_{002} peak of the graphite at $2\theta = 26.1^\circ$ indicated an interlayer spacing of 0.336 nm and after oxidation this characteristic graphite peak disappeared and was replaced by a well defined peak at $2\theta = 10.9^\circ$ with 0.81 nm d-spacing. This increased d-spacing of GO sheets was due to the presence of abundant oxygen-containing functional groups on both sides of the graphene sheet.

For the mGOi, the position and relative intensities of all diffraction peaks at 2θ values of 18.27° (111), 30.1° (220), 35.4° (311), 43.05° (400), 56.94° (422), 62.51° (511), and 73.95° (553) were consistent with the standard XRD data for the spinel structure Fe_3O_4 with lattice constants of $\alpha = 8.397$ Å (indexed using Joint Committee on Power Diffraction Standards database (JCPDS 19-0629)).[25] The average crystallite size D (nm) of the Fe_3O_4 particles was calculated using the known Debye–Sherrer equation.[26] The average size of the Fe_3O_4 particles using 35.56° diffraction peak was found to be ~18.4 nm.

The (001) diffraction peak of GO at 10.3° totally disappeared, suggesting that the layered GO has been exfoliated in the preparation process of mGOi nanocomposite. The absence of the peak at $2\theta = 10.3^\circ$, suggested the complete exfoliation of graphite oxide during the preparation process, while a broad small peak at $2\theta = 24.4^\circ$ (002) corresponding to the graphene sheets indicated the formation of the Fe_3O_4/GO nanocomposites.

The XRD pattern of the mGOp was different. It appeared to be amorphous, may be due to the effect of the ammonia solution. However, wide peaks were observed at $2\theta = 30.1^\circ$ and ~57.2° that were attributed to (220) and (511) of Fe_3O_4 and a small peak at $2\theta = 24.4^\circ$ (002) corresponding to the graphene sheets, indicating the formation of the magnetic composite.

According to the SEM image of the mGOi nanoparticles, the nanosize of particles prepared was evident. Furthermore, the iron

distribution map of mGOi, indicated that Fe was well distributed in the prepared magnetic composite.[16] Differences in the chemistry of the surfaces of the prepared nanocomposites have been seen on the differential thermal gravimetric (DTG) curve measured in nitrogen, where the peaks represented weight loss at the specific temperature range and the area under the peaks was related to the extent of that weight loss; the mGOp curve is compared with the DTG curve of graphene oxide.

The first peak centered at about 80–100°C for all samples, correlated with the endothermic effect on the differential thermal analysis (DTA) curves, was linked to the weight loss due to evaporation of physically adsorbed water. In the case of the mGOp composite, that peak presented a maximum at 100°C. The exothermic peak at 200–250°C (presented on the DTA curve for the GO sample) was related to decomposition of epoxy and carboxyl groups. This peak was no longer observed for the mGOi nanocomposite since the layered GO had been exfoliated in the preparation process of graphene oxide and mGOi nanocomposite, while only a small peak was presented for the mGOp sample, maybe due to some small residue of GO.

For this sample a significant part of the weight loss at temperatures above 750°C had to be related to the gradual dehydration/dehydroxylation of iron oxyhydroxides.[27] Their formation during the co-precipitation synthetic route has been reported.[28] Nevertheless, that their existence was not testified by XRD may be due to the amorphous appearance of the XRD pattern of this magnetic material. These oxyhydroxides were finally reduced in two steps to metallic iron between 750 and 900°C, and from the weight loss curve it was concluded that their percentage was about 22%. No weight loss occurred for the mGOi samples above 530°C.

The magnetization hysteresis loop of mGOi and mGOp nanocomposites (at room temperature) was also examined. The magnetization curves were S-like curves and presented zero coercivity and permanence indicating the superparamagnetic property of the nanocomposite. The saturation magnetization of the mGOi magnetic adsorbent was found to be about 65 emu g^{-1}, while the respective value of mGOp was considerably smaller. The latter was attributed to the smaller percentage of magnetite in this sample, due to the formation of iron oxyhydroxides, as seen by DTA measurements. In both cases, the saturation magnetization was strong enough for convenient magnetic separation. A characteristic image of an aqueous dye solution is shown as Fig. 2 before adsorption on mGOp and then after separation, in the presence of an external magnetic field; the black particles of the magnetic composite were attracted to the wall of the vial.[16]

Fourier transform infrared spectroscopy (FTIR) of the parent graphite oxide and the prepared nanocomposites were studied.[16] All samples presented the O–H stretching vibration adsorption band at 3424 cm^{-1} and the band at ~1600 cm^{-1}, which was attributed to C=C stretching mode of the sp^2 carbon skeletal network. Carboxyl groups of GO were observed as bands at 1720 cm^{-1} and 1380 cm^{-1} as the stretching vibration peaks of carboxyl and carbonyl, while the bands at 1055 cm^{-1} and 1230 cm^{-1} were attributed to the stretching vibrations of C–O of epoxy groups. The C=O groups were thought to facilitate the attachment of magnetic nanoparticles through a covalent coupling or electrostatic interaction.[29]

The spectra of mGOi and mGOp nanocomposites additionally presented the characteristic stretching vibration peak at 568 cm^{-1} which proved that Fe_3O_4 nanoparticles were successfully anchored

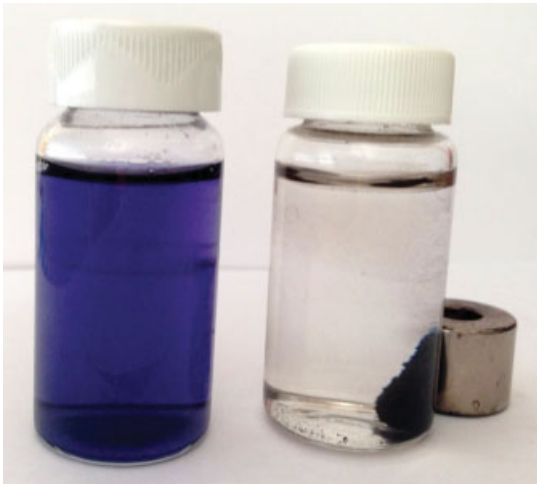

Figure 2. Image of the magnetic graphene oxide nanoparticles (synthesized by co-precipitation) adsorbing RB5 dye; on the right, following magnetic separation. Reprinted with permission; copyright MDPI AG (2012).[16]

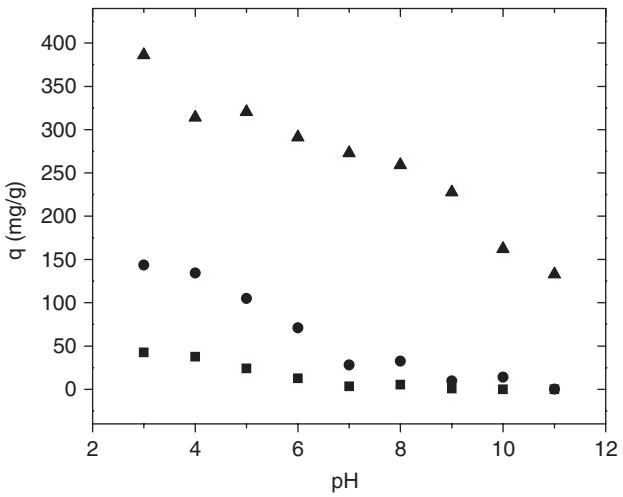

Figure 3. Effect of pH on adsorption capacity of tetracycline. Graphene oxide 0.181 mg mL^{-1}; initial concentration of tetracycline: 8.33 (■), 33.33 (●), 166.67 mg L^{-1} (▲). Reprinted with permission; copyright Elsevier (2012).[34]

onto their graphene sheets. These materials also presented adsorption peaks related to oxygen-containing functional groups, but at decreased intensity, maybe due to the formation of –COO– after coating with Fe_3O_4.[30] So, it was concluded that Fe_3O_4 nanoparticles were chemically deposited on GO with the aid of the –COOH on GO. The mGOp nanocomposite presented an additional band at 1400 cm^{-1}, which represented the vibrations of nitrogen in NH_4^+ inorganic ion; this was reported to be a Brönsted acid, which can react with deprotonated carboxylic type acidic sites to form ammonium salts, or become adsorbed as NH_4^+ on the metal acidic sites.[31]

On the other hand, the presence of iron favours Lewis acid–base interactions, offering/contributing in this way binding sites for ammonium ions. This band did not appear after dye adsorption due to reaction of these ions with the sulphonate groups of the dye. In the case of GO, the shift of the band was indicative that the binding of dye (RB5) molecules was predominant, based on the

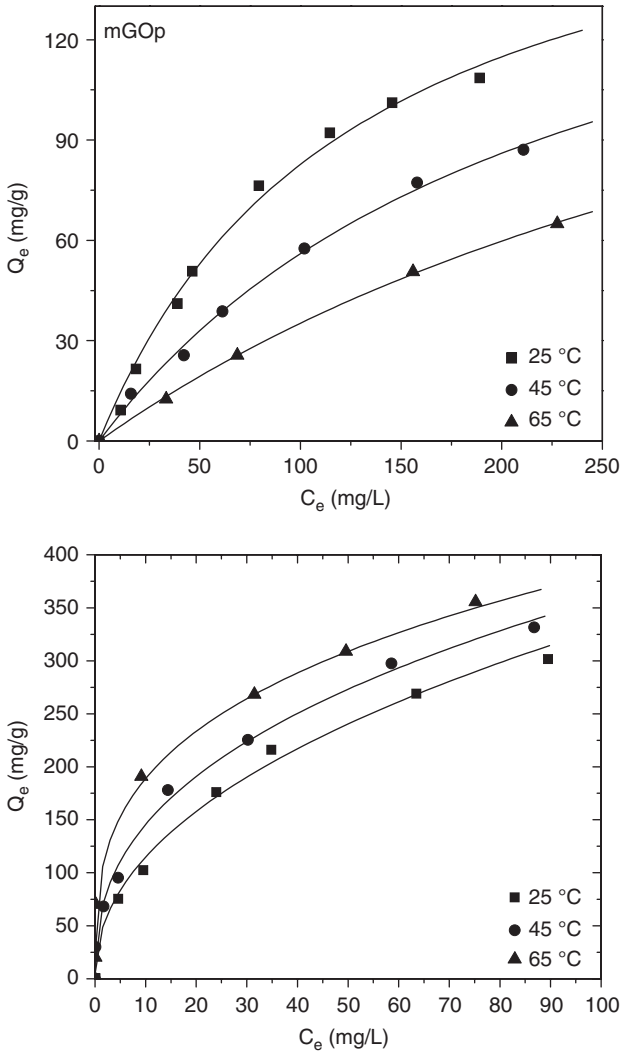

Figure 4. Isotherms of the adsorption of RB5 dye on magnetic grapheme oxide nanoparticles, synthesized by co-precipitation (top) and onto graphite oxide/magnetic chitosan nanocomposite (bottom). Reprinted with permission; copyright MDPI AG (2012) and ACS (2013), respectively.[16,32]

$\pi-\pi$ interaction between the aromatic ring of the dye and the GO basal planes.[32]

ORGANICS

The extensive use of tetracycline antibiotics has caused a lot of environmental pollution and for this reason, GO functionalized magnetic particles were prepared and utilized as adsorbents for rapid removal of four such samples (tetracycline, oxytetracycline, chlortetracycline, and doxycycline) from aqueous solution.[33] Highly efficient removal performance was found for low levels of antibiotics in large volumes of water solutions, applied also to Pearl River water. A higher adsorption capacity was measured, and also calculated by the Langmuir model.[34] Some of the results are shown in Fig. 3; GO was used as an adsorbent, owing to its excellent hydrophilicity. The kinetics of adsorption were fitted to the pseudo-second-order model, while the mechanism for tetracycline adsorption on GO was deduced to be via $\pi-\pi$ interaction and cation-π bonding.

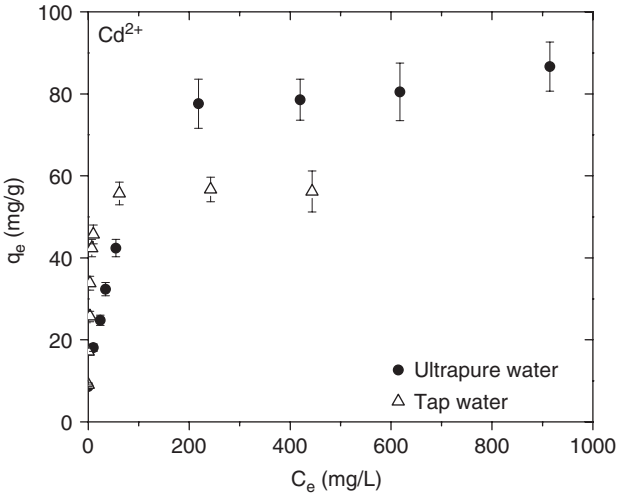

Figure 5. Adsorption curves for cadmium (pH 6, contact time 24 h, adsorbent dosage 1 g L^{-1}). Reprinted with permission; copyright Elsevier (2013).[41]

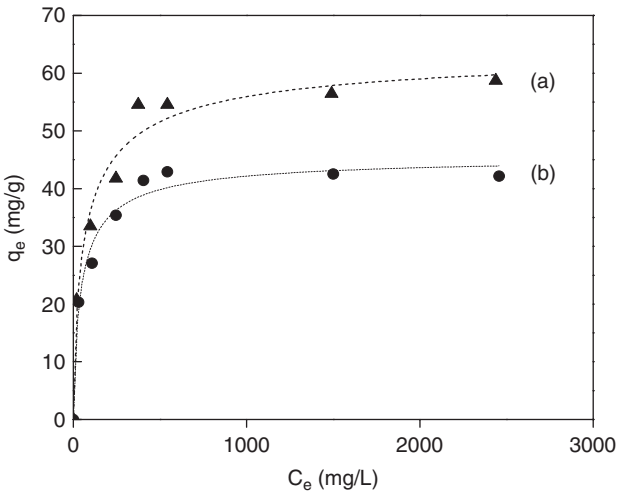

Figure 6. Adsorption isotherms of copper ion onto gel beads of (a) calcium alginate and (b) also with encapsulated GO. Reprinted with permission; copyright Elsevier (2013).[45]

Carbon-based nanomaterials (which have unique π-electronic structure) have been used as excellent adsorbents for the removal of aromatic compounds, an area that has become a hot research topic; RGO/iron oxide composites were prepared to adsorb 1-naphthylamine, 1-naphthol and naphthalene with different polarities.[35] Electron donor–acceptor interaction was proposed to be the primary mechanism and the adsorption capacity increased with increasing dipole moment. Thermodynamic experiments further indicated that the process was endothermic and spontaneous.

Magnetic cyclodextrin-chitosan/GO with high surface area was synthesized via a simple method and examined for the removal of hydroquinone from simulated wastewater.[36] The process was found to obey the Freundlich adsorption model and its kinetics followed a pseudo-second-order rate equation. The removal mechanism of this adsorbent was thought to be the electrostatic adsorption of hydroquinone in the form of negatively charged hydroquinone by positively charged chitosan, accompanying

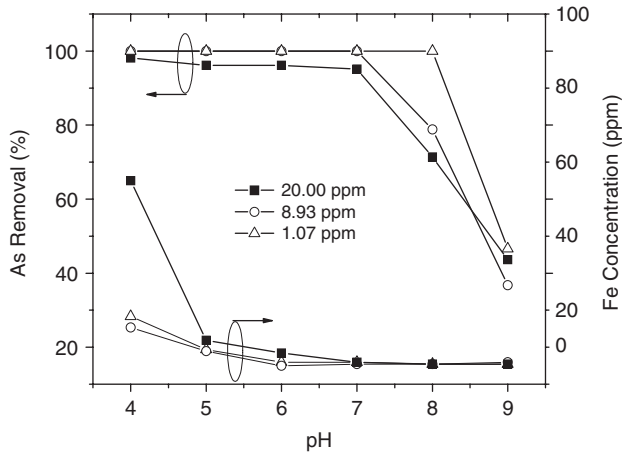

Figure 7. Effects of pH on arsenate removal at different initial concentration and the ferric concentration in the filtrate. Reprinted with permission; copyright Elsevier (2010).[49]

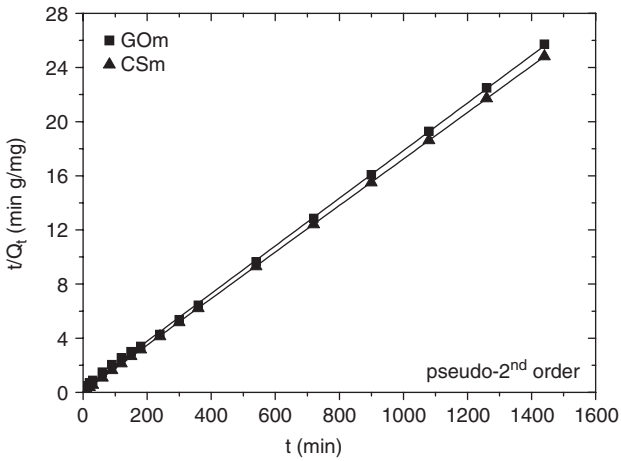

Figure 9. Effect of contact time on adsorption of mercury ions onto magnetic GO and cross-linked chitosan: fitting to the pseudo-second-order kinetic equation. Presented recently at a national (Greek) conference.[23]

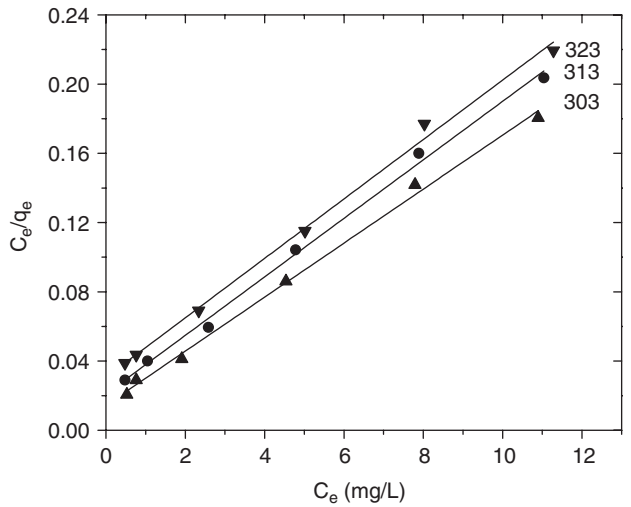

Figure 8. Isotherms (Langmuir) for chromium removal (magnetic cyclodextrin-chitosan/GO = 1.0 g L^{-1}, pH 3). Reprinted with permission; copyright Elsevier (2013).[53]

Table 1. Adsorption of mercury(II) onto magnetic graphene oxide[23]

C_0 (mg L^{-1})	T (K)	q_e (mg g^{-1})
20	298	14.02
	318	15.06
	338	16.98
100	298	56.02
	318	60.08
	338	62.99
500	298	123.10
	318	145.04
	338	150.03

hydroquinone absorbed by cavities of the cyclodextrin, and forming hydrogen bonds between hydroquinone and the hydroxyl groups on the surface.

Adsorption of two synthetic organic compounds (phenanthrene and biphenyl) by two pristine graphene nanosheets and one GO was examined, and compared with those of a coal base activated carbon, a single-walled carbon nanotube, and a multi-walled carbon nanotube, in distilled and deionized water and in the presence of natural organic matter.[37] Graphenes exhibited comparable or better adsorption capacities than carbon nanotubes and granular activated carbon, which was attributed to a much less compact bundle structure. The impact of natural organic matter on the adsorption of synthetic organic compounds was smaller on graphenes. The results indicated that graphenes can serve as alternative adsorbents for removing organic compounds from water. A photocatalyst, magnetic TiO_2–graphene, was designed and facilely produced by combining sol–gel and assembling processes; taking advantages of graphene and TiO_2, the catalyst exhibited strong light absorption in the visible region and high adsorption capacity for organic pollutants (herbicides).[38]

GO was also employed for the removal of commonly occurring algal toxins, such as microcystin-LR and microcystin-RR from water.[39] The adsorption performance of GO was compared with that of commercially available activated carbon. In recent years, there has been a rapid increase in the frequency of occurrence of algal blooms all over the world, due to an excessive supply of nutrients resulting from urbanization and industrialization. GO could be reused as an adsorbent following ten cycles of adsorption/desorption with no significant loss in its adsorption capacity.

Figure 4 presents a comparison of the adsorption of the Reactive Black 5 dye. The shapes of curves indicate that the isotherms for the adsorbent–dye systems studied are I-Type, according to the BET classification, and characterized by a high degree of adsorption at low concentrations.[16] At higher concentrations, the available adsorption sites become fewer and subsequently the adsorption depends on the initial concentration of dye. From a thermodynamic point of view, the adsorption process was enthalpy driven ($\Delta S^0 < 0$). The negative values of the standard Gibbs free energy also showed the spontaneous adsorption of reactive dyes on the adsorbent. An increase was found in the negative value of ΔG^0 with an increase in temperature, implying that lower temperature was making adsorption easier. The negative value of ΔH^0 indicated the exothermic nature of

the process; thereby demonstrating that the process was stable energetically.

The results for the GO[16] were fitted well to the Langmuir model and showed calculated maximum adsorption capacities for RB5 removal at 25°C (pH = 3) to be 164, and 188 mg g^{-1} for mGOi, and mGOp, respectively. On the other hand, at the same conditions a q_{max} of 221 mg g^{-1} for graphite oxide and 391 mg g^{-1} for graphite oxide functionalized with magnetic chitosan were reported.[32] In this case, the material characterization indicated that a significant fraction of chitosan amines: (i) were inserted between the graphite oxide layers; and (ii) reacted with carboxyl and epoxy groups of graphite oxide, leading to its reduction and hence, the destruction of the layered structure.

Information about the differences in the chemistry of the surfaces was seen in the differential thermal gravimetry curves.[32] Also, the interactions of the adsorbent–dye system were confirmed by FTIR spectroscopy through shifts of the peaks occurring after dye adsorption. For the same dye, a hydrophilic and biocompatible three-dimensional (3D) chitosan–graphene structure, with large specific surface area and unique mesoporosity, was prepared and tested efficiently.[40]

A more general study by Wang and co-workers presents recent literature data for the use of GO as an organic compounds adsorbent, but not in the liquid phase.[12] In this study, the removal of some gas pollutants (VOCs) demonstrated the ability of GO to act both in gaseous and aqueous media.

HEAVY METALS

Heavy metal and ionic dyes commonly often co-exist and so constitute an important and dangerous source of environmental pollution; the results of this work[41] (here, also with Methylene blue and Orange G adsorbed onto a GO nanocomposite) showed that the kinetic data followed a pseudo-second-order model and the equilibrium data were well fitted to the Langmuir model (Fig. 5). In a mono-component system, the maximum adsorption capacity in ultrapure water for Cd^{2+} was 91.29 mg g^{-1}. Comparable results for the maximum adsorption capacity were obtained earlier for cadmium biosorption.[42] The effects of pH, ionic strength, and humic acid on Cd^{2+} and Co^{2+} sorption on few-layered graphene oxide nanosheets were investigated elsewhere.[43]

Magnetic chitosan grafted with GO sheets, which showed increased surface area, was used as adsorbent for the removal of Pb^{2+} ions from large volumes of aqueous solutions.[44] The abundant functional groups on the adsorbent surface played an important role in metal ion adsorption. Equilibrium studies showed that the data for Pb^{2+} adsorption followed the Langmuir model and the maximum adsorption capacity for Pb^{2+} was estimated to be 76.94 mg g^{-1}. Adsorption capacities of activated carbons prepared from various materials towards Pb^{2+} ions have recently been presented in a comparative table.[8]

The performance of calcium alginate with encapsulated GO gel beads for the removal of Cu^{2+} ions from aqueous solution was studied (Fig. 6).[45] The adsorption isotherm data were fitted by Langmuir isotherms and the kinetics data were described by a pseudo-second-order kinetic equation. While the increased oxygen functionalities on GO led to more adsorption capacity compared with calcium alginate alone, the adsorption process at these sites was slower. Another technique, biosorptive flotation, has been attempted[46] for the simultaneous abstraction of nickel, copper and zinc ions in lab-scale batch as well as pilot-scale continuous experiments; from the three metal ions investigated, copper was the first and best adsorbed.

Zinc ion removal by iron-based adsorbents was also examined.[47] The maximum capacity for Zn^{2+}, adsorbed effectively by GO, was reported to be up to 246 mg g^{-1} with a Langmuir adsorption equilibrium constant of 5.7 L g^{-1} (at 20°C).[48] The thermodynamic parameters calculated from temperature-dependent sorption isotherms suggested that Zn^{2+} sorption on GO was an exothermic and spontaneous process in nature.

A series of composites based on graphene oxide cross-linked with ferric hydroxide was developed for the removal of arsenate from contaminated drinking water (Fig. 7).[49] The adsorption of an anion depends on acid/base properties of the adsorbent surfaces, and the specific interactions between the adsorbate and the surface functional groups on the adsorbents. Arsenic, among the heavy metals species, is known for its marked negative impacts on human health because of its chronic and carcinogenic effects as well as acute lethality. Drinking water contamination by arsenic remains a major public health problem around the world, especially in Bangladesh, India, USA, China, Mexico, Chile, Greece, etc.

The role of carbon surface chemistry and structural heterogeneity on iron oxyhydroxide and thus, on the adsorption of arsenate have been published recently.[50] It is noteworthy to say that the research experience of our lab on pentavalent and trivalent arsenic removal has been highlighted in a Special issue of a journal, entitled 'Metal ions removal from liquid effluents' and guest edited by one of the authors (Professor K.A. Matis).[51] The highest adsorption capacity (328 mg g^{-1}) corresponded to surfactant-modified akaganéite (i.e. b-FeOOH).

Another metal, commonly identified as hazardous contaminant because of its high toxicity, mobility and bioaccumulation is certainly hexavalent chromium; calcined graphene/MgAl-layered double hydroxides,[52] and GO functionalized with magnetic cyclodextrin-chitosan (Fig. 8)[53] were successfully tested for this case. Layered double hydroxides are known suitable adsorbents for chromates removal.[54] Of course, another alternative is biosorption.[55]

Figure 9 and Table 1 present some of the results obtained for mercury ion removal by GO;[23] a thermodynamics study was also included. A theoretical maximum adsorption capacity of 121 mg g^{-1} was obtained for Hg^{2+} ion using natural zeolites in industrial tests.[56]

CONCLUDING REMARKS

The published results are of importance for the environmental application of graphene oxide nanocomposites (based on GO advantages) for the enrichment and removal of inorganic and organic compounds/pollutants from large volumes of aqueous solutions and effluents. The magnetic separation of the loaded adsorbent could also contribute to convenient solid–liquid separation, required downstream. Further research is warranted.

REFERENCES

1 Jacoby M, Graphene moves toward applications: as composites and inks become commercial products, advanced electronics remain a long way off. *Chem Eng News* **89**:10–15 (2011).
2 Alvarez LH and Cervantes FJ, (Bio)nanotechnologies to enhance environmental quality and energy production. *J Chem Technol Biot* **86**:1354–1363 (2011).
3 Kemp KC, Seema H, Saleh M, Le NH, Mahesh K, Chandra V and Kim KS, Environmental applications using graphene composites: water remediation and gas adsorption. *Nanoscale* **5**:3149–3171 (2013).

4 Zhang N, Qiu H, Si Y, Wang W and Gao J, Fabrication of highly porous biodegradable monoliths strengthened by graphene oxide and their adsorption of metal ions. *Carbon* **49**:827–837 (2011).
5 Freundlich H, Over the adsorption in solution. *Z Phys Chem* **57**:385–470 (1906).
6 Langmuir I, The adsorption of gases on plane surfaces of glass, mica and platinum. *J Am Chem Soc* **40**:1361–1403 (1918).
7 Smith JM and Van Ness HC, *Introduction to Chemical Engineering Thermodynamics*, 4th edn. McGraw-Hill, New York (1987).
8 Deliyanni E, Arabatzidou A, Tzoupanos N and Matis K, Adsorption of Pb2+ using mesoporous activated carbon and its effects on surface modifications. *Adsorp Sci Technol* **30**:627–645 (2012).
9 Karapantsios TD, Loukidou MX and Matis KA, Sorption kinetics, in *Water Encyclopedia*, Wiley, Hoboken NJ, 564–569 (2005).
10 Ho YS and McKay G, A comparison of chemisorption kinetic models applied to pollutant removal on various sorbents. *Process Safety Environ Protect* **76**:332–340 (1998).
11 Azizian S, Kinetic models of sorption a theoretical analysis. *J Colloid Interface Sci* **276**:47–52 (2004).
12 Wang S, Sun H, Ang HM and Tadé MO, Adsorptive remediation of environmental pollutants using novel graphene-based nanomaterials. *Chem Eng J* **226**:336–347 (2013).
13 Brodie BC, On the atomic weight of graphite. *Philos Trans Royal Soc London* **149**:249–259 (1859).
14 Staudenmaier L, Verfahren zur Darstellung der Graphitsäure. *Berichte der deutschen chemischen Gesellschaft* **31**:1481–1487 (1898).
15 Hummers Jr WS and Offeman RE, Preparation of graphitic oxide. *J Am Chem Soc* **80**:1339 (1958).
16 Kyzas GZ, Travlou NA, Kalogirou O and Deliyanni EA, Magnetic graphene oxide: effect of preparation route on reactive black 5 adsorption. *Materials* **6**:1360–1376 (2013).
17 Massart R, Preparation of aqueous magnetic liquids in alkaline and acidic media. *IEEE Trans Magnetics* **MAG-17**:1247–1248 (1981).
18 Giakisikli G and Anthemidis AN, Magnetic materials as sorbents for metal/metalloid preconcentration and/or separation. *A review. Anal Chim Acta* **789**:1–16 (2013).
19 Sreeprasad TS, Maliyekkal SM, Lisha KP and Pradeep T, Reduced graphene oxide–metal/metal oxide composites: facile synthesis and application in water purification. *J Hazard Mater* **186**:921–931 (2011).
20 Mao S, Pu H and Chen J, Graphene oxide and its reduction: modeling and experimental progress. *RSC Adv* **2**:2643–2662 (2012).
21 Kassaee MZ, Motamedi E and Majdi M, Magnetic Fe3O4-graphene oxide/polystyrene: fabrication and characterization of a promising nanocomposite. *Chem Eng J* **172**:540–549 (2011).
22 Li J, Zhou SI, Hong G-B and Chang C-T, Hydrothermal preparation of P25–graphene composite with enhanced adsorption and photocatalytic degradation of dyes. *Chem Eng J* **219**:486–491 (2013).
23 Kyzas GZ, Travlou NA, Matis KA and Deliyanni EA, On the kinetics and thermodynamics of mercury(II) removal from aquoeus solutions with magnetic graphene oxide and magnetic chitosan. *Proceedings of 9th Panhellenic Sci Conf Chem Eng* (Athens, Greeece) (2013).
24 Kyzas GZ, Kostoglou M, Vassiliou AA anad Lazaridis NK, Treatment of real effluents from dyeing reactor: experimental and modeling approach by adsorption onto chitosan. *Chem Eng J* **168**:577–585 (2011).
25 Wang C, Feng C, Gao Y, Ma X, Wu Q and Wang Z, Preparation of a graphene-based magnetic nanocomposite for the removal of an organic dye from aqueous solution. *Chem Eng J* **173**:92–97 (2011).
26 Seung HH, Thermal reduction of graphene oxide, in *Physics and Applications of Graphene - Experiments*, ed by Mikhailov S. InTech, Rijeka, Croatia, 73–90 (2011).
27 Deliyanni E and Bandosz TJ, Importance of carbon surface chemistry in development of iron-carbon composite adsorbents for arsenate removal. *J Hazard Mater* **186**:667–674 (2011).
28 Kanel SR, Manning B, Charlet L and Choi H, Removal of arsenic(III) from groundwater by nanoscale zero-valent iron. *Environ Sci Technol* **39**:1291–1298 (2005).
29 Rattana, Chaiyakun S, Witit-anun N, Nuntawong N, Chindaudom P, Oaew S, Kedkeaw C and Limsuwan P, Preparation and characterization of graphene oxide nanosheets. *Procedia Eng* **32**:759–764 (2012).
30 Bai L-Z, Zhao D-L, Xu Y, Zhang J-M, Gao Y-L, Zhao L-Y and Tang J-T, Inductive heating property of graphene oxide–Fe3O4 nanoparticles hybrid in an AC magnetic field for localized hyperthermia. *Mater Lett* **68**:399–401 (2012).
31 Huang CC, Li HS and Chen CH, Effect of surface acidic oxides of activated carbon on adsorption of ammonia. *J Hazard Mater* **159**:523–527 (2008).
32 Travlou NA, Kyzas GZ, Lazaridis NK and Deliyanni EA, Functionalization of graphite oxide with magnetic chitosan for the preparation of a nanocomposite dye adsorbent. *Langmuir* **29**:1657–1668 (2013).
33 Lin Y, Xu S and Li J, Fast and highly efficient tetracyclines removal from environmental waters by graphene oxide functionalized magnetic particles. *Chem Eng J* **225**:679–685 (2013).
34 Gao Y, Li Y, Zhang L, Huang H, Hu J, Shah SM and Su X, Adsorption and removal of tetracycline antibiotics from aqueous solution by graphene oxide. *J Colloid Interface Sci* **368**:540–546 (2012).
35 Yang X, Li J, Wen T, Ren X, Huang Y and Wang X, Adsorption of naphthalene and its derivatives on magnetic graphene composites and the mechanism investigation. *Colloid Surface A* **422**:118–125 (2013).
36 Li L, Fan L, Sun M, Qiu H, Li X, Duan H and Luo C, Adsorbent for hydroquinone removal based on graphene oxide functionalized with magnetic cyclodextrin-chitosan. *Int J Biol Macromol* **58**:169–175 (2013).
37 Apul OG, Wang Q, Zhou Y and Karanfil T, Adsorption of aromatic organic contaminants by graphene nanosheets: comparison with carbon nanotubes and activated carbon. *Water Res* **47**:1648–1654 (2013).
38 Tang Y, Zhang G, Liu C, Luo S, Xu X, Chen L and Wang B, Magnetic TiO2-graphene composite as a high-performance and recyclable platform for efficient photocatalytic removal of herbicides from water. *J Hazard Mater* **252–253**:115–122 (2013).
39 Pavagadhi S, Tang ALL, Sathishkumar M, Loh KP and Balasubramanian R, Removal of microcystin-LR and microcystin-RR by graphene oxide: adsorption and kinetic experiments. *Water Res* **47**:4621–4629 (2013).
40 Cheng J-S, Du J and Zhu W, Facile synthesis of three-dimensional chitosan–graphene mesostructures for reactive black 5 removal. *Carbohyd Polym* **88**:61–67 (2012).
41 Deng J-H, Zhang X-R, Zeng G-M, Gong J-L, Niu Q-Y and Liang J, Simultaneous removal of Cd(II) and ionic dyes from aqueous solution using magnetic graphene oxide nanocomposite as an adsorbent. *Chem Eng J* **226**:189–200 (2013).
42 Loukidou MX, Karapantsios TD, Zouboulis AI and Matis KA, Diffusion kinetic study of cadmium(II) biosorption by Aeromonas caviae. *J Chem Technol Biotechnol* **79**:711–719 (2004).
43 Zhao G, Li J, Ren X, Chen C and Wang X, Few-layered graphene oxide nanosheets as superior sorbents for heavy metal ion pollution management. *Environ Sci Technol* **45**:10454–10462 (2011).
44 Fan L, Luo C, Sun M, Li X and Qiu H, Highly selective adsorption of lead ions by water-dispersible magnetic chitosan/graphene oxide composites. *Colloid Surface B* **103**:523–529 (2013).
45 Algothmi WM, Bandaru NM, Yu Y, Shapter JG and Ellis AV, Alginate–graphene oxide hybrid gel beads: an efficient copper adsorbent material. *J Colloid Interface Sci* **397**:32–38 (2013).
46 Zouboulis AI, Lazaridis NK and Matis KA, Removal of toxic metal ions from aqueous systems by biosorptive flotation. *J Chem Technol Biotechnol* **77**:958–964 (2002).
47 Deliyanni EA, Peleka EN and Matis KA, Removal of zinc ion from water by sorption onto iron-based nanoadsorbent. *J Hazard Mater* **141**:176–184 (2007).
48 Wang H, Yuan X, Wu Y, Huang H, Zeng G, Liu Y, Wang X, Lin N and Qi Y, Adsorption characteristics and behaviors of graphene oxide for Zn(II) removal from aqueous solution. *Appl Surf Sci* **279**:432–440 (2013).
49 Zhang K, Dwivedi V, Chi C and Wu J, Graphene oxide/ferric hydroxide composites for efficient arsenate removal from drinking water. *J Hazard Mater* **182**:162–168 (2010).
50 Deliyanni E, Bandosz TJ and Matis KA, Impregnation of activated carbon by iron oxyhydroxide and its effect on arsenate removal. *J Chem Technol Biotechnol* (2012).
51 Deliyanni EA, Peleka EN, Gallios GP and Matis KA, A critical review of the separation of arsenic oxyanions from dilute aqueous solution (the contribution of LGICT). *Int J Environ Waste Manage* **8**:286–304 (2011).
52 Yuan X, Wang Y, Wang J, Zhou C, Tang Q and Rao X, Calcined graphene/MgAl-layered double hydroxides for enhanced Cr(VI) removal. *Chem Eng J* **221**:204–213 (2013).
53 Li L, Fan L, Sun M, Qiu H, Li X, Duan H and Luo C, Adsorbent for chromium removal based on graphene oxide functionalized

with magnetic cyclodextrin–chitosan. *Colloid Surface B* **107**:76–83 (2013).
54 Lazaridis NK, Pandi TA and Matis KA, Chromium(VI) Removal from aqueous solutions by Mg-Al-CO3 hydrotalcite: sorption-desorption kinetic and equilibrium studies. *Ind Eng Chem Res* **43**:2209–2215 (2004).
55 Loukidou MX, Zouboulis AI, Karapantsios TD and Matis KA, Equilibrium and kinetic modeling of chromium(VI) biosorption by *Aeromonas caviae*. *Colloid Surface A* **242**:93–104 (2004).
56 Chojnacki A, Chojnacka K, Hoffmann J and Górecki H, The application of natural zeolites for mercury removal: from laboratory tests to industrial scale. *Mineral Eng* **17**:933–937 (2004).

